Pergamon

PII: S0967-0645(96)00037-9

Deep-Sea Research II, Vol. 43, No. 7-8, pp. 1683-1712, 1996

0967-0645/96 $15.00 + 0.00

Turbulence dissipation rates and nitrate supply in the upper water column on Georges Bank

EDWARD P. W. HORNE,* JOHN W. LODER,* CHRISTOPHER E. NAIMIE† and NEIL S. OAKEY*

(*Received* 13 *October* 1994; *in revised form* 29 *January* 1996; *accepted* 7 *May* 1996)

Abstract—Measurements of velocity microstructure in the upper water column on Georges Bank are used to contrast the summertime structure of turbulent kinetic energy dissipation rate between the central mixed area and the tidal-mixing front, and to compare vertical nitrate fluxes with frontal-zone primary production demands. In the mixed area during weak winds, the dissipation rate varies strongly over the semidiurnal tidal period in close relation to the tidal current strength, varies with the monthly/fortnightly tidal modulation, and generally increases with distance below the sea surface. Collectively, these features provide strong support for the elevated vertical mixing rates on Georges Bank being primarily due to the tides, although wind forcing also contributes significantly. In the frontal zone on northern Georges Bank, the upper-ocean dissipation rates are about an order of magnitude weaker than in the mixed area, have a more complex temporal variation during the tidal period, and also vary with the monthly/fortnightly tidal modulation. The vertical eddy flux of nitrate into the frontal euphotic zone varies over the tidal period and with the tidal modulation. Averaged over the tidal period, the estimated fluxes are about one-third of the nitrogen demand estimated from concurrent primary production measurements, supportive of an important contribution from turbulent mixing to new production in the frontal zone, but also pointing to additional processes and/or inadequate data coverage of this complex zone. The measured dissipation rates at both the mixed and frontal sites are in approximate agreement with the turbulence levels in two 3-D numerical models for summertime tidal and mean circulation on the Bank, one with an eddy-viscosity and the other an advanced turbulence closure. The latter model has more realistic vertical turbulence distributions and indicates strong sensitivity of the turbulence levels to horizontal position in the frontal zone.

INTRODUCTION

Areas in which water mass properties remain vertically well-mixed year-round are a common feature of tidally-energetic shallow seas (e.g. Simpson *et al.*, 1977; Garrett *et al.*, 1978; Schumacher *et al.*, 1979; Bowman *et al.*, 1983). Such areas are generally attributed to turbulent mixing in the bottom boundary layer of strong tidal flows, largely on the basis of increased current magnitudes and rough agreement between the areas' spatial extent and the predictions of Simpson and Hunter's (1974) "depth/dissipation" criterion (see Simpson and Sharples (1994) for a recent re-examination using an advanced turbulence closure model). However, few measurements of turbulence levels in the upper water column in such areas,

* Department of Fisheries and Oceans, Bedford Institute of Oceanography, P.O. Box 1006, Dartmouth, N.S., Canada B2Y 4A2.

† Thayer School of Engineering, Dartmouth College, Hanover, NH 03755, U.S.A.

and of the relationship of these levels to tidal current strength or other possible forcings, have been reported (Soulsby, 1983; Dewey and Crawford, 1988; Veth, 1990).

The occurrence of a year-round "mixed" area on Georges Bank (Fig. 1) has been recognized and attributed to tidal mixing for seventy years (e.g. Bigelow, 1927). Garrett *et al.* (1978) showed that the summertime extent of this and other mixed areas in the Gulf of Maine is in rough agreement with the Simpson and Hunter (1974) criterion for tidal mixing. However, Loder and Greenberg (1986) pointed out that other criteria, which either make different assumptions about the vertical structure of tidal mixing or also include a contribution from wind mixing, provide comparable agreement with the observations. Thus, the relative contributions of tidal and wind forcing to vertical mixing on Georges Bank, as well as the absolute mixing rates and their spatial and temporal variability, have not been firmly established. Recently, Bisagni and Sano (1993) have provided firm support for a dominant influence from tidal mixing, with evidence of a low-frequency variation in surface temperature associated with the monthly and fortnightly tidal modulations.

Associated with the mixed areas are summertime "tidal-mixing" fronts, the transition zones between the mixed areas and the adjacent stratified deeper waters where currents are generally weaker (e.g. Simpson, 1981). Considering the assumed origin of such fronts, a strong cross-frontal variation in the intensity of vertical mixing is expected. This mixing has been hypothesized to be a critical factor in the high primary production at tidal(-mixing) fronts, contributing to optimal conditions of light and nutrient supply (e.g. Pingree, 1978). Recent observations (Horne *et al.*, 1989; Harrison *et al.*, 1990; Loder *et al.*, 1992b) of enhanced "new" primary production (based on inorganic nitrogen) at the Georges Bank tidal front suggest that frontal processes play a fundamental role in the Bank's rich fisheries production.

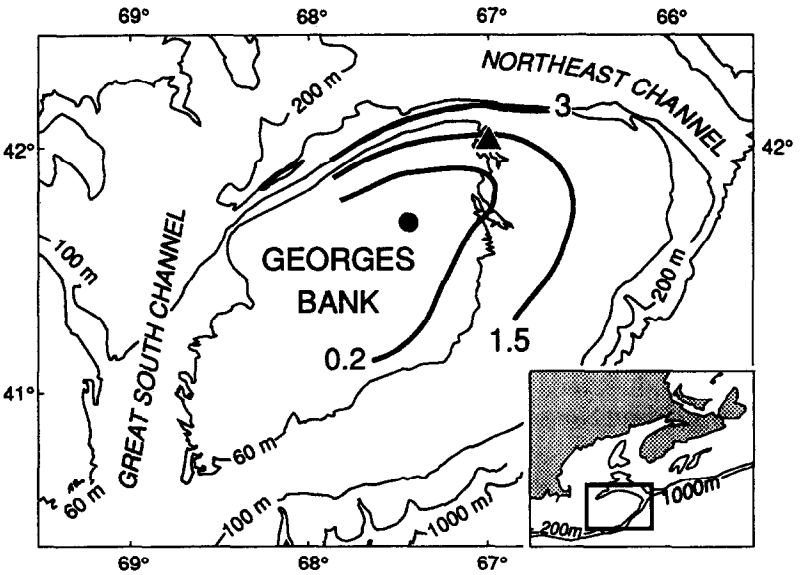

Fig. 1. Location and bathymetric map for Georges Bank showing the mixed (●) and frontal (▲) sites, and the density difference (in σ_t units) between the surface and 50 m from a CTD survey (Horne *et al.*, 1989) during the study period.

Modern instrumentation, such as profilers mounted with shear probes from which rates of turbulent kinetic energy dissipation can be estimated (e.g. Osborn, 1980; Dewey *et al.*, 1987; Oakey, 1988), provides the capability of measuring turbulence levels in tidally-mixed and frontal areas. In addition to their application to various biological and dispersion problems, such observations are important for addressing a number of physical oceanographic questions regarding tidally generated turbulence and its interrelation with circulation and stratification. These include: the structure and generation mechanisms of the turbulence; the magnitude and parameterization of bottom and internal friction in tidal and residual circulation models; and the associated variations in water mass properties.

In this paper we describe turbulence dissipation rate measurements taken in July–August 1985 as part of a field study of frontal mixing and primary production on Georges Bank (see Horne *et al.*, 1989 for background on the study). Using the profiler EPSONDE (Oakey, 1988), velocity microstructure in the upper two-thirds of the water column was measured over the semidiurnal tidal period at two sites: a "mixed" site on the central Bank where stratification influences were negligible, and a "frontal" site on the Bank's northern side. The mixed-site observations serve as a homogeneous-fluid benchmark for the vertical and temporal structure of the dissipation rate, while the frontal-zone measurements provide information on this structure in the presence of stratification. The primary objectives here are to: (i) describe the magnitude, and spatial and temporal structure of dissipation rate in the upper water column on Georges Bank, contrasting the mixed area and frontal zone; and (ii) to evaluate whether the vertical nutrient fluxes associated with turbulent mixing in the Georges Bank frontal zone are adequate to support measured primary production rates. This examination complements a more extensive study of frontal-zone physics and biology carried out in 1988 (Loder *et al.*, 1992a, 1992b, 1993; Tremblay and Sinclair, 1992; Brickman and Loder, 1993; Perry *et al.*, 1993; Yoshida and Oakey, 1996) which did not include concurrent turbulence and primary production measurements, nor turbulence measurements in the central mixed area.

We start with brief descriptions of the instrumentation used in the study, the observational strategy and procedure, and the analysis procedure used to estimate dissipation rates. In the following two sections, we present the dissipation rates for the mixed and frontal sites respectively, with emphases on the vertical structure averaged over the tidal period and the temporal variability of the vertical-averaged rate for specified vertical intervals. The results are then interpreted, including comparison with the turbulence energy levels in the Naimie *et al.* (1994) and Naimie (1995, 1996) numerical circulation models for Georges Bank, estimation of the contributions from wind forcing, and discussion of the implications for vertical eddy diffusivities. In the subsequent section, the computed diffusivities are used to estimate vertical nitrate fluxes for comparison with those required by the primary production measurements described in Horne *et al.* (1989).

METHODS

Instrumentation

Profiles of velocity microstructure were obtained using the instrument EPSONDE (Oakey, 1988) mounted with two airfoil shear probes (e.g. Osborn and Crawford, 1980) and other sensors. The shear probes measure high-frequency (in effect, high-wavenumber) fluctuations in the vertical gradient of horizontal velocity, from which the dissipation rate of

turbulent kinetic energy can be estimated. During operation, EPSONDE fell vertically at 0.7–1.0 m/s with its sensors leading and out of the wake of the profiler. A slack, multi-conductor tether transferred the data to a shipboard data logger and facilitated profiler retrieval and repeated profiling. Because EPSONDE did not have a bottom-impact probe guard during the 1985 study, the microstructure profiles extended only from the surface to 15–20 m above the seafloor (and thus did not cover the core of the bottom boundary layer).

Observations of the background hydrographic and velocity fields were obtained using a Guildline Model 8705 CTD unit and an Aanderaa current meter lowered from the research vessel. Water samples for nutrient analyses were taken from rosette bottles at selected CTD stations. In addition, a subsurface mooring with Aanderaa current meters (with temperature and conductivity sensors) at depths of 13, 33 and 53 m was deployed at the frontal-zone site (water depth 63 m), but it was struck by a fishing vessel prior to completion of the study and only the 13- and 33-m instruments were recovered. During microstructure sampling, hourly or bi-hourly wind velocity from the ship's anemometer was also recorded.

The measurements of carbon assimilation rate, nitrate and ammonia uptake rates, and other biological and chemical variables are described in Horne *et al.* (1989).

Observational strategy and program

The field measurements were obtained on northeastern Georges Bank (Fig. 1) between 24 July and 11 August 1985 (Table 1). A Eulerian observational strategy, involving measurements over a tidal period at two fixed locations, was adopted. To minimize the influence of horizontal variations in stratification and tidal currents, the mixed site was chosen to be at least one tidal excursion (about 10 km) away from the tidal front and major topographic features, although depth variations of the order 5 m were observed. Thus, all water columns observed at the site during a particular tidal period were expected to have similar (negligible) stratification and to have experienced similar tidal and wind forcing. In contrast, there were large horizontal variations in stratification and water depth within a tidal excursion of the frontal site, as well as internal waves providing an additional turbulence forcing (e.g. Loder *et al.*, 1993).

The microstructure measurements were obtained by dropping EPSONDE from the stern of the research vessel while anchored at each site. Groups or "bursts" of microstructure profiles were taken at approximately 90-min intervals, typically over a semidiurnal tidal period. Each sampling burst consisted of 4–6 profiles at 2–4 min intervals, to obtain information on short-term variability in the turbulence. During the 0.5–1 min period of each drop, EPSONDE and the sampled water column were advected 50–100 m astern by the strong current. Three "anchor stations" (B, D, E) at the mixed site and two (A, F) at the frontal site yielded useful data over the tidal period under different tide and wind conditions (Table 1). The number of drops per burst and the frequency of bursts varied when sensor or instrument repairs were required. Observations within 5 m of the sea surface were not included in the analyses due to probable contamination by the ship's wake and/or initial wobbling of the falling instrument.

Most microstructure sampling bursts were preceded or followed by a CTD cast and a current profile using the Aanderaa meter. At the frontal site, nutrient samples were taken at 10-m intervals during the CTD up-casts. The profiling current meter was held for three 30-s instrument cycles at nominal depths of 10, 20, 30, 40 and 50 m below the surface. Observations were taken on both the down- and up-casts so that the total profile time was

Table 1. *Position, water depth, time and other information on the five anchor stations which yielded useful microstructure data*

	A	B	D	E	F
N latitude	42° 6.8′	41° 43.1′	41° 42.8′	41° 43.2′	42° 6.9′
W longitude	67° 1.9′	67° 30.0′	67° 29.9′	67° 30.1′	67° 2.6′
Water depth (m)	63	48	53	55	63
Station type	F	M	M	M	F
Start date	25 July	26 July	2 August	10 August	11 August
Start time (UTC)	0442	2212	2057	2155	1205
Duration (h)	13+	12	9+	10+	12
Tidal elevation range at Yarmouth (m)	3.4	3.4	3.6	2.5	2.3
Current measurements:					
No. profiles	4	9	11	9	8
No. moored meters	2	—	—	—	—
Average current speed (m/s)	0.64	0.64	0.60	0.43	0.43
Average wind speed (m/s)	6	12	7	2	3
Microstructure measurements:					
No. bursts	9	8	9	9	8
No. profiles	48	48	46	53	47
Average dissipation rate ($\times 10^{-7}$ W/kg)					
9–29 m	3.0	45.7	20.5	11.2	1.9
9–35 m	3.4	—	20.8	13.8	2.0
9–41 m	3.4	—	—	—	2.3

Station type refers to frontal (F) or mixed (M). The tidal elevation range is the average difference between high and low tides during the anchor station, as predicted by the Canadian Hydrographic Service. The current speed is the tidal-averaged magnitude of the vertical-averaged velocity for the 20–40 m interval from the profiling current meter, except for A where it is the tidal-averaged magnitude of the average of the 13- and 33-m moored measurements. The wind speed is the average of hourly observations from the ship's anemometer on CSS Hudson.

about 20 min. Observations at depths of 12 m and less were not included in the final analysis because of apparent degradation of the direction measurements by the ship's magnetic field. Biological profile measurements were taken approximately twice daily during the study period (Horne *et al.*, 1989).

During anchor station A at the frontal site, the vessel was approximately 1 km from the current meter mooring. The 5-min recording interval of the current meters provided a continuous record of the currents and stratification in the upper water column.

Data analysis procedure

The microstructure dataset typically consisted of profiles of two (orthogonal) components of velocity shear broken into approximately 1.5-m segments for analysis. Using established spectral techniques (Oakey, 1982) the shear variance, σ_{sh}^2, was estimated for each segment (with corrections for instrument noise and sensor response). The rate of turbulent kinetic energy dissipation, ε, was then calculated (Hinze, 1959) as $\varepsilon = 7.5\upsilon\sigma_{sh}^2$ (W/kg), where υ is the kinematic viscosity of seawater.

Each profile of turbulence dissipation rate was converted to a common format consisting of 2-m vertical bins centered on even depths (in m). For a particular anchor station, the

resulting dataset was an array $\varepsilon(z,t)$, where z is the depth (below the surface) and t is time. Three arithmetic averaging operators were used in the examination of temporal and vertical structure. In each case, the standard deviation (SD) about the mean was retained as an indicator of the variability within the subset, and the standard error (SE = SD/$\sqrt{N}$) of the mean as a crude indicator of the statistical significance of differences among the means (note, however, that this SE is not a reliable statistic for dissipation rate, which generally has a skewed distribution (e.g. Gurvich and Yaglom, 1967; Yamazaki and Lueck, 1990)):

1. A "burst-averaged" profile, $\bar{\varepsilon}(z, t)$, was computed as the mean of the 4–6 individual profile values for each vertical bin. (The associated standard deviations and errors then reflect "intraburst" temporal variability including contributions from the advection of small-scale spatial structures.)
2. A "tidal-averaged" profile, $\tilde{\varepsilon}(z)$, for each anchor station was computed as the mean of the burst-averaged values for each bin in order to examine vertical structure averaged over the tidal period. (The associated standard deviations and errors then reflect "tidal" and other "interburst" variability in the burst-averaged dissipation rates.)
3. A vertical/burst average, $\hat{\varepsilon}(t)$, was computed as the burst average of the vertical average of $\varepsilon(z,t)$ over a common vertical interval in order to simplify the examination of temporal variability during the tidal period. (The standard deviations and errors of the vertical/burst means then reflect intraburst variability in the vertical-averaged dissipation rate.)

The profiling current meter data were reduced to a single profile for each station, by averaging the down-cast observations in the vicinity of the nominal depths and assigning the average to the average depth of observation. Current estimates at specified levels were then obtained from linear interpolation or extrapolation.

The CTD and moored current measurements were processed routinely, except for the computation of salinity for the 13-m current meter. Since salinity computed from the raw temperature and conductivity had spurious spikes, apparently arising from the non-simultaneous (seconds) sampling and different sensor time constants in combination with the high-frequency internal wave field, salinity was alternatively computed from the (current-meter) temperature time series and a conductivity–temperature regression relation determined from the 13-m observations.

RESULTS FOR "MIXED" SITE

Current structure

Currents at the mixed site were dominated by the semidiurnal tidal current, as illustrated by the results (Fig. 2) of regression analysis of the current components to a constant term plus 12.4 h sinusoid. There is considerable similarity in the current structure at anchor stations D and E, during which winds were relatively weak (Table 1), with the tidal current shear indicating that the bottom boundary layer occupied much of the water column. The stronger currents at D are consistent with the occurrence of stronger tides during this station (Table 1), supporting limited wind influences at both D and E.

In contrast, the tidal and mean currents at B have a different vertical structure, and the north–south component of the tidal current is amplified compared to D and E. These differences appear to be associated primarily with the occurrence of stronger winds during

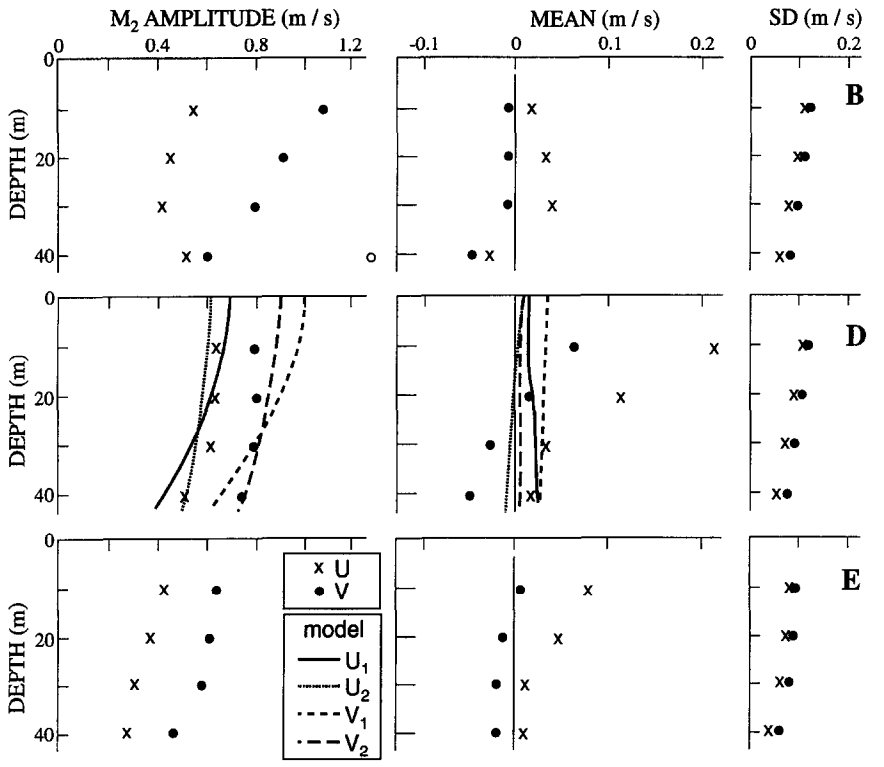

Fig. 2. Tidal current amplitudes, mean currents and standard deviations (×, •) (between observations and predictions) from regressions of a constant term plus 12.4-h sinusoid to the observed currents for anchor stations B, D and E at the mixed site. The observed currents are the profiling meter observations interpolated/extrapolated to 10-m depth levels. The profiles of M_2 current amplitude and mean current from the Naimie *et al.* (1994; U_1, V_1) and Naimie (1996; U_2, V_2) circulation models are included on the station D panels (without adjustments for depth and tidal modulation). The current components are for an east (U)–north (V) co-ordinate system.

B, although it appears that the temporal variations due to tides and wind during this station are not adequately separated by the regression analysis.

Intraburst dissipation rate variability

Individual profiles of the dissipation rate for a representative microstructure sampling burst during anchor station E at the mixed site are shown in Fig. 3. Typical errors associated with each data point are expected to be of the order $\pm 50\%$. The profiles show vertical structure on scales ranging from the profile depth to a few meters, with little coherence in the smaller-scale variations between successive profiles. This is consistent with the expectation that small-scale turbulence is patchy in space and highly intermittent in time. The large variability exhibited by this burst of 6 profiles over a time interval of less than 30 min is the motivation for our "burst" sampling, which improves the statistical stability of the dissipation rate estimates by ensemble averaging.

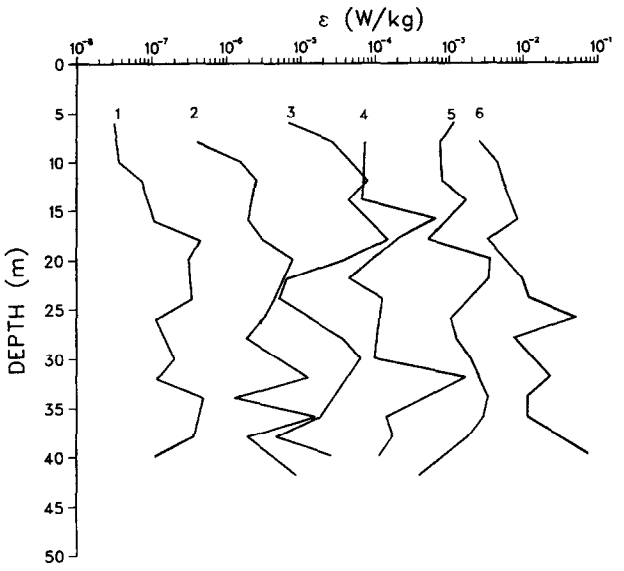

Fig. 3. Individual profiles of dissipation rate for a typical burst at the mixed site (hour 7.51 of anchor station E; Fig. 4). Successive profiles are offset (to the right) by one order of magnitude.

Temporal and vertical distribution of burst-averaged rates

The variability of the burst-averaged dissipation rate profiles, $\bar{\varepsilon}(z,t)$, at the mixed site is illustrated in Fig. 4 for the anchor station (E), which has the best coverage and lowest average wind speed (Table 1). The dominant feature is a temporal variation of more than an order of magnitude during the tidal period (cf. hours 3.86 and 8.93), which indicates that the small-scale turbulence on Georges Bank develops and decays on a timescale of hours or less. There is again substantial vertical structure on scales ranging from the profile depth to a few meters, with rates generally increasing with depth (z) and little interburst coherence apparent for the small-scale structure.

The burst-averaged dissipation rates from the three mixed-site anchor stations (Table 1)

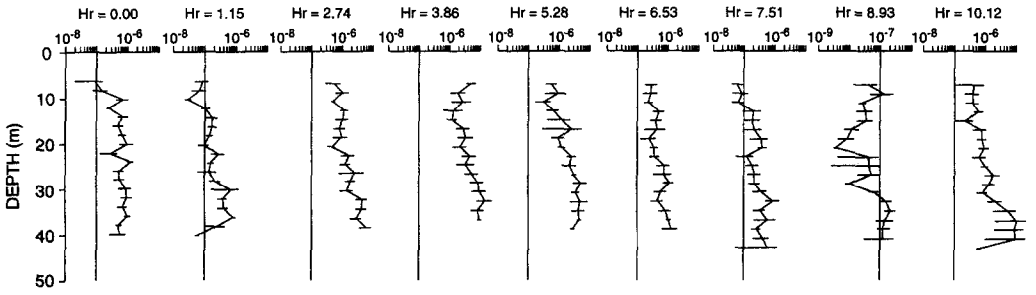

Fig. 4. Successive profiles of burst-averaged dissipation rate ($\bar{\varepsilon}$) during anchor station E. The horizontal bars indicate ± 1 standard error of the burst average. The vertical line in each profile corresponds to $\bar{\varepsilon} = 10^{-7}$ W/kg.

are contrasted in Fig. 5 using time-depth (t–z) contour plots of $\bar{\varepsilon}(z,t)$. Substantial vertical and strong temporal variability is present at all stations. A notable feature of the t–z distributions of $\bar{\varepsilon}$ is the lack of any noticeable vertical phase shift in the development and disappearance of high-dissipation features, indicating that temporal variability over the tidal period involves rapid expansion and contraction of the bottom boundary layer.

An indication of variability among the mixed-site anchor stations on timescales longer than the semidiurnal tidal period is provided by the vertical average of the tidal-averaged dissipation rates for some common vertical intervals (Table 1). The highest tidal-averaged dissipation rate occurred during B when both tides and wind were relatively strong. The dissipation rate at D was approximately one-half of that at B, while that at E was smaller again, consistent with decreased tides and winds (see the subsection "Influence of Wind Forcing" for further discussion).

Vertical structure averaged over tidal period

Although Figs 4 and 5 indicate that the dissipation rate varies considerably in time, the average profile over the tidal period is used in many applications (e.g. frontal position criteria, mean circulation models). The tidal-averaged profiles, $\tilde{\varepsilon}(z)$, for the three mixed-site anchor stations are considerably smoother than the burst-averaged profiles and generally show a monotonic increase with z (Fig. 6). The reduced small-scale structure is consistent with the intermittent and patchy nature of turbulence and the requirement for considerable averaging to obtain stable statistics. The greater vertical structure at D (than B or E) is associated with the occurrence in the 11–13 m bin at station 227 (hour 5.5 of D in Fig. 5) of the highest burst-averaged dissipation rate for any depth in the entire anchor station, which may indicate that our sampling frequency is still not fully adequate. Nevertheless, linear regression analysis indicates a statistically significant (95% level) overall increase in tidal-averaged dissipation rate with depth for all three anchor stations.

Temporal variation of vertical-averaged rates, and relation to current indices

The strong temporal variation over the tidal period is further illustrated by time series plots (Fig. 7) of the vertical/burst-averaged dissipation rates $\hat{\varepsilon}(t)$ over common vertical intervals in which there is a burst sample for all bins (and below 9 m to avoid any ship's wake influence). There are variations in $\hat{\varepsilon}$ exceeding an order of magnitude at all three mixed-site anchor stations, with a suggestion of a component near the second harmonic (6.2 h) of the M_2 tidal period. Regression analysis to a constant term plus 6.2-h sinusoid confirms a highly significant (99% level) second-harmonic variation at B and D, and a variation significant at the 93% level at E. These results support the suggestion that small-scale turbulence on Georges Bank is largely driven by the tides, since the second harmonic variation is consistent with the dominant variations in current speed and current shear magnitude for an elliptical semidiurnal tidal current with eccentricity near 0.7 (Fig. 2).

The relation of the dissipation rate variability to potential forcing indices is displayed in Fig. 7. Two indices computed from the current profile data are considered: (i) the magnitude of the vertical-averaged velocity, as a measure of the strength of the current regime; and (ii) the magnitude of the vertical (vector) difference in velocity, as a measure of the vertical shear. These quantities are computed for the 20–40 m interval because of the degradation of the near-surface current measurements. The variation in $\hat{\varepsilon}$ is similar to the variation in both

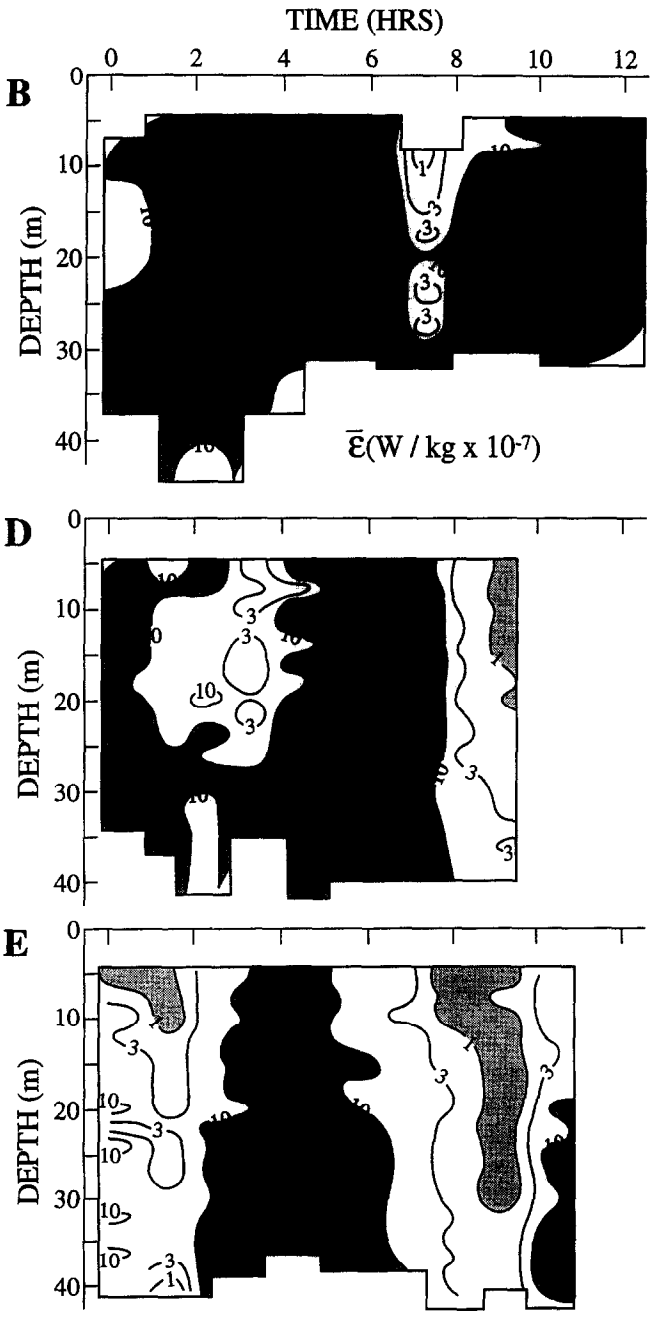

Fig. 5. Time–depth plots of $\bar{\varepsilon}$ for anchor stations B, D and E at the mixed site. The time origins are the start times in Table 1. Values above 10^{-6} W/kg are indicated by dark shading and those below 10^{-7} W/kg by light shading.

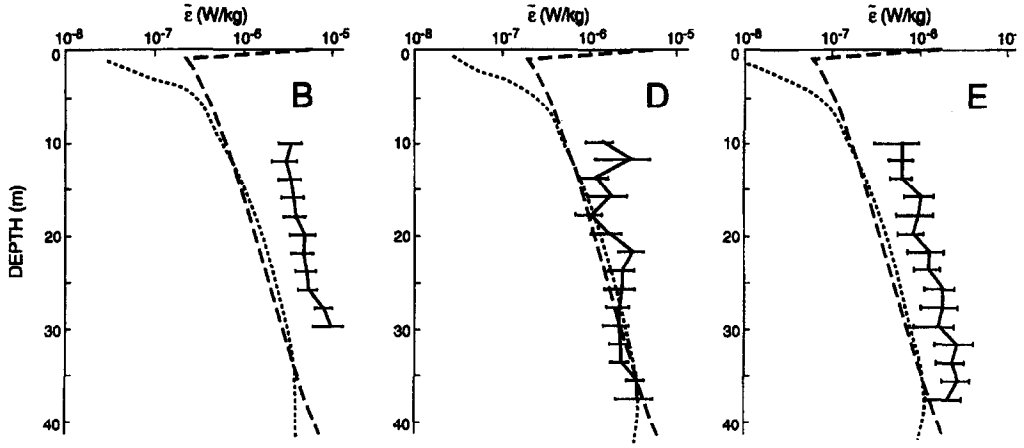

Fig. 6. Profiles (solid curves) of tidal-averaged dissipation rate ($\bar{\varepsilon}$) for anchor stations B, D and E. Averages are shown for vertical bins away from any ship's wake influence (i.e. below 9 m) and with data from at least six bursts. The horizontal bars indicate ± 1 standard error of the tidal average computed from the burst averages. The adjusted (for depth and tidal modulation) turbulence energy production rates estimated from the Naimie *et al.* (1994) model (dotted curves) and the adjusted dissipation rates from the Naimie (1996) model (dashed curves) are also shown. The model values have been adjusted by the factors 1.26, 1.1 and 0.34 for B, D and E, respectively.

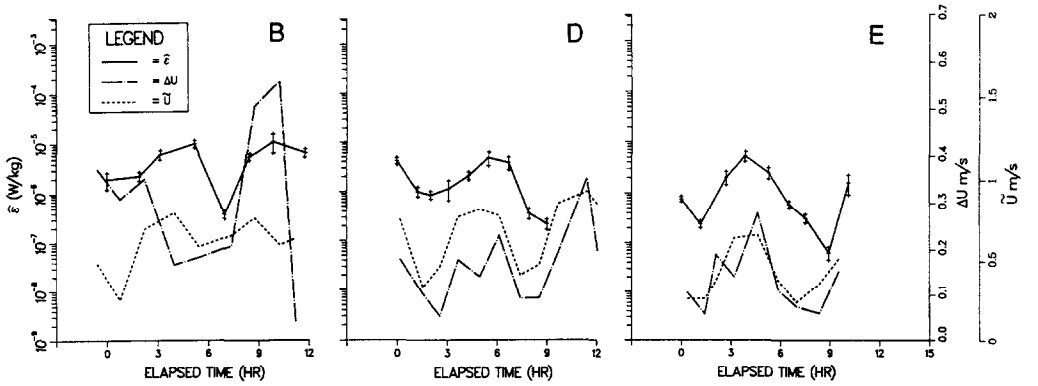

Fig. 7. Time series plots of the vertical/burst-averaged dissipation rate ($\hat{\varepsilon}$), magnitude of depth-averaged current ($\tilde{U}$) and magnitude of vertical difference in velocity (ΔU) for anchor stations B, D and E. The time origins are the start times in Table 1, and the vertical bars through the $\hat{\varepsilon}$ values indicate ± 1 standard error of the burst average computed from the vertical averages. The vertical intervals for the dissipation rates are 9–29 m for B, and 9–35 m for D and E. The current indices are for the 20–40 m interval.

the vertical-averaged current magnitude and the vector velocity difference at D and E. In particular, the phase lags of an hour or less (unresolvable with the present burst separation) suggest a short timescale for the turbulence cascade from the energy input scales to the dissipation scales. In contrast, there is much less similarity between the dissipation rate variations and the measured currents at B, probably due to an increased wind influence that is not represented in the currents measured below the near-surface region.

Regression analyses were used to explore the functional relation between $\hat{\varepsilon}$ and the current indices in Fig. 7, using first- and second-degree polynomials in the current indices, and linear relations with the square and cube of these indices. The analyses indicate highly significant (95% level) statistical relationships between the dissipation rate and both current indices for D and E but not B. However, the data are not adequate to determine the exact relationship or better forcing index. Regressions using $\hat{\varepsilon}$ and current indices for 19–35 m, the largest interval common to both the dissipation and current measurements, generally give similar results. The observations thus indicate that, at least in the absence of strong winds (stations D and E), the mixed-area dissipation rates have a strong dependence on local current strength and/or vertical shear. However, further measurements are required to determine the best parameterization of the dissipation rates.

RESULTS FOR "FRONTAL" SITE

Dissipation rate magnitudes, and current and density structure

The dissipation rates observed at the stratified frontal site (Fig. 1) on the northern side of Georges Bank may now be contrasted with those described above from the mixed site. As indicated by the vertical averages of the tidal-averaged rates for the various anchor stations (Table 1), the frontal-site dissipation rates (stations A and F) are about an order of magnitude lower than those at the mixed site. It appears that the origin of this large difference is not principally related to the current regime, since the measured currents at the two sites (Figs 2 and 8; Table 1) are comparable. The lower turbulence levels at the frontal

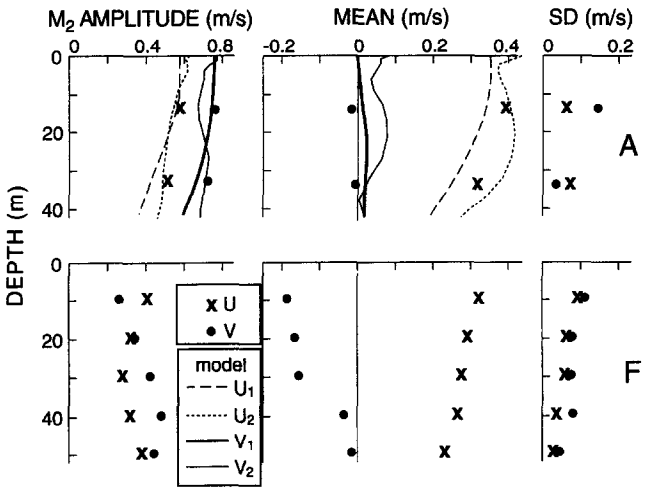

Fig. 8. Tidal current amplitudes, mean currents and standard deviations (×, •) (between observations and predictions) from regressions of a constant term plus 12.4-h sinusoid to the observed currents for anchor stations A and F at the frontal site. The observed currents for A are from the moored meters, and for F are from the profiling meter observations interpolated/extrapolated to 10-m depth levels. The profiles of M_2 current amplitude and mean current from the Naimie *et al.* (1994; U_1, V_1) and Naimie (1996; U_2, V_2) circulation models are included on the panels for station A (without adjustments for depth and tidal modulation). The current components are for an east (U)–north (V) co-ordinate system, which is approximately along/cross-frontal.

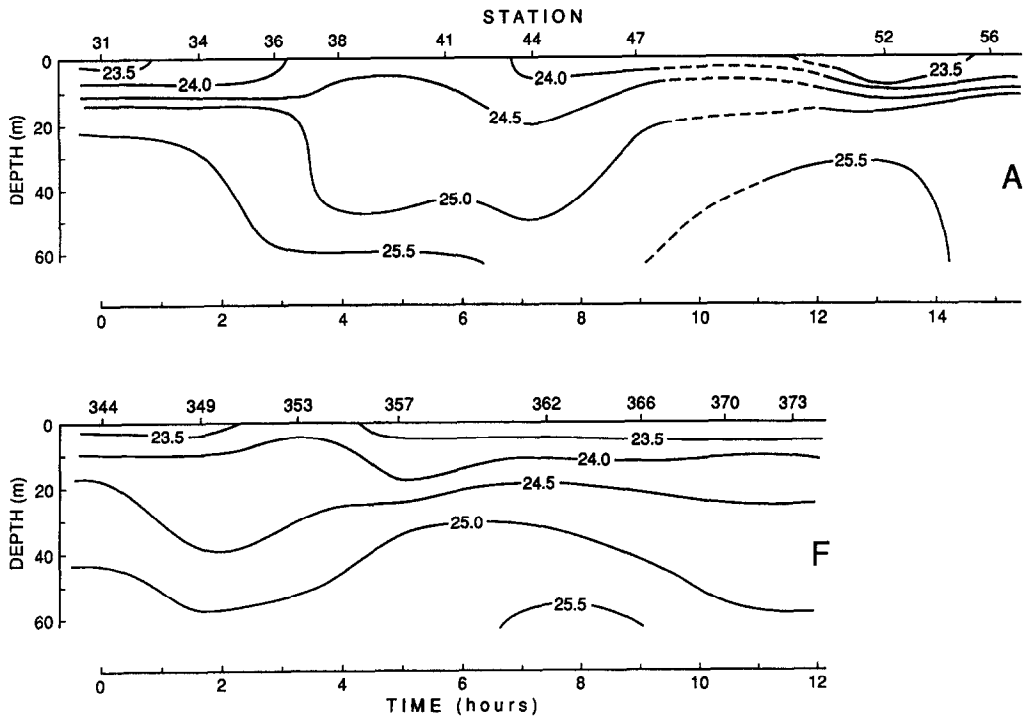

Fig. 9. Time–depth plots of density (σ_t units) from CTD profiles during anchor stations A and F. The time origins are 0401 UTC, 25 July for A and 1146 UTC, 11 August for F.

site are probably associated with the substantial stratification (e.g. Loder *et al.*, 1993), illustrated in *t–z* plots (Fig. 9) of the density structure obtained from the CTD profiles. The stratification is persistent but varies during the tidal period, primarily as a result of advection of the front by the strong tidal currents (Loder and Horne, 1991; Loder *et al.*, 1992a).

Comparison of the vertical averages of the tidal-averaged rates for A and F (Table 1) also indicates a longer-term variation in the dissipation rate at the frontal site. Like that at the mixed site, this variation is qualitatively consistent with the monthly/fortnightly tidal modulation (Table 1, Fig. 8). The density field (Fig. 9) also shows a smaller variation in stratification over the tidal period during weaker tides (station F), consistent with reduced tidal advection.

Intraburst and interburst dissipation rate variability

Individual profiles (not shown) indicate that the instantaneous ε field in the frontal zone also has vertical structure on scales ranging from the profile depth to a few meters. However, more structure on the 10-m scale, and increased coherence in this structure between adjacent profiles than at the mixed site are apparent.

The variability of the burst-averaged dissipation rates ($\bar{\varepsilon}$) from the two frontal anchor stations is illustrated in the *t–z* plots of Fig. 10. The rates exhibit greater vertical structure and lower vertical coherence of their temporal variations than those at the mixed site, in

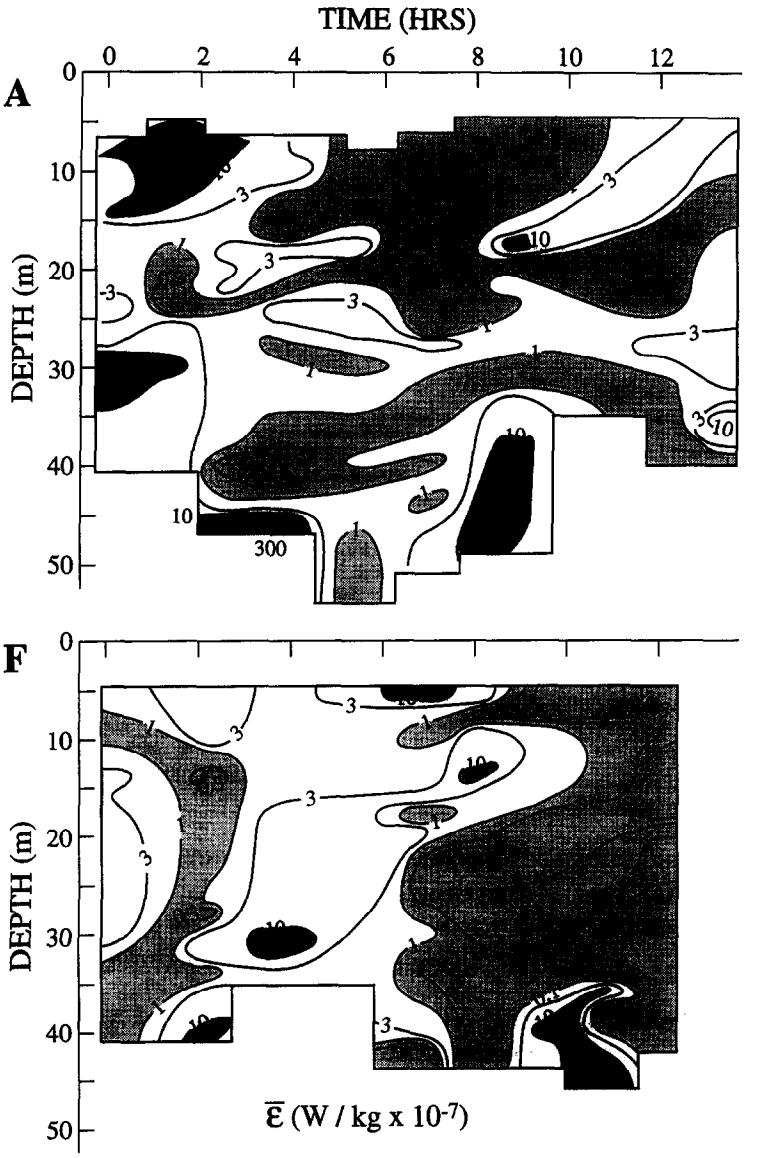

Fig. 10. Time–depth plots of $\bar{\varepsilon}$ for anchor stations A and F at the frontal site (otherwise, as in Fig.

addition to the lower magnitudes. "Tidal" variability in the dissipation rate is less apparent than at the mixed site, and not obviously related to the variation in stratification (Fig. 9). It can be seen from Figs 5 and 10 that the highest burst-averaged dissipation rate at either site occurred at 48 m at station A, consistent with high dissipation rates at the frontal site being more confined to the near-bottom region (as observed in the 1988 study (Loder *et al.*, 1993) and predicted by advanced turbulence models (see subsection "Comparison with Turbulence Energy Levels in 3-D Numerical Models")).

Vertical structure averaged over tidal period

The vertical profiles of tidal-averaged dissipation rate ($\bar{\varepsilon}$) for stations A and F (Fig. 11) have more small-scale structure than those at the mixed site (Fig. 6). A vertical trend is no

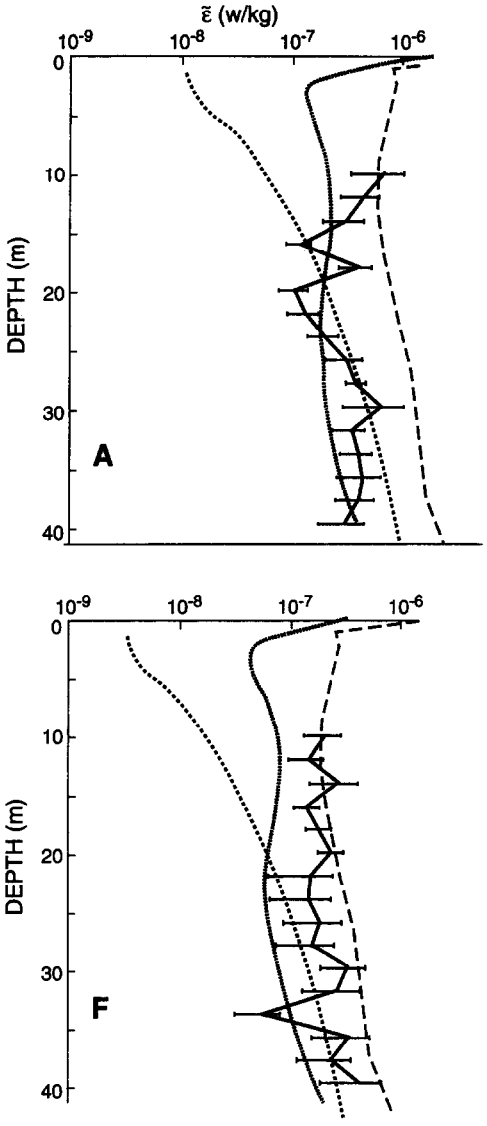

Fig. 11. Profiles (solid curves) of tidal-averaged dissipation rate ($\bar{\varepsilon}$) for anchor stations A and F (criteria and format as in Fig. 6). The adjusted (for depth and tidal modulation) turbulence energy production rates estimated from the Naimie *et al.* (1994) model (wide-spaced dotted curves), and adjusted dissipation rates for two positions ("similar h" — dashed curve; "same lat./long."—close-spaced dotted curve) in the Naimie (1996) model are also shown. The adjustment factors are 1.03 and 0.32 for A and F, respectively, for the similar h nodes, and 1.81 and 0.56 for the same lat./long. positions.

longer apparent, and regression analysis confirms that, over the sampled portion (9–41 m) of the frontal zone, there is no significant increase or decrease of the tidal-averaged dissipation rate with depth.

Temporal variation of vertical-averaged rates, and relation to current and density indices

Time series plots (Fig. 12) of the vertical/burst-averaged dissipation rates ($\hat{\varepsilon}$) at the frontal site indicate less temporal variability over the tidal period in the vertically-averaged rate than at the mixed site. A significant variation at the second harmonic (6.2 hour) of the semidiurnal tide is neither apparent nor suggested by regression analysis. The variability in $\hat{\varepsilon}$ shows only limited similarity to the variations in vertical-averaged velocity magnitude, magnitude of vertical difference in velocity and vertical difference in density (Fig. 12). Regression analyses using first- and second-degree polynomials, and quadratic and cubic relations indicate no significant correlations (at the 95% level) with the current and density indices.

Several factors may contribute to the lower tidal variation in dissipation rate at the frontal site (than at the mixed site), and the absence of a correlation with the current and density indices. First, the current measurements and other studies (e.g. Loder *et al.*, 1992a) point to a more complex (baroclinic) current regime in the frontal zone: the stronger mean current (Figs 2 and 8) gives both the current strength and vertical shear a different temporal variation than at the mixed site (also see next subsection), and the current strength and shear (Fig. 12) are not as closely related as at the two mixed-site stations with relatively-weak winds (Fig. 7). Second, although the winds were weak during both stations A and F (Table 1), it is possible that the wind contribution to dissipation rate in the upper water column was relatively more important because of the weaker overall dissipation rates. Third and perhaps most importantly, internal waves generated along the northern edge of the Bank can contribute significantly to turbulence in the frontal zone (Brickman and Loder, 1993; Loder *et al.*, 1992a, 1993; Yoshida and Oakey, 1996). An indication of the occurrence of internal waves during A is provided in Fig. 13, which shows time series of temperature and north–south (cross-bank) current at the 13-m level. Large fluctuations in temperature, similar to the signatures of various internal waveforms found in the more intensive 1988 study (Brickman and Loder, 1993; Loder *et al.*, 1992a), are apparent. This supports internal waves as an important additional source of turbulent mixing in the frontal zone, thereby complicating its temporal variability (Yoshida and Oakey, 1996). The present observations, nevertheless, indicate that the dissipation rates in the upper water column of the frontal zone are about an order of magnitude weaker than in the mixed area, and have a different temporal and vertical structure.

INTERPRETATION AND IMPLICATIONS OF DISSIPATION RATES

Comparison with turbulence energy levels in 3-D numerical models

Comparison of measured turbulence dissipation rates with the turbulence distributions predicted by numerical circulation models is important to both the field validation of the models and the critical evaluation of assumptions and procedures in turbulence measurements. In this subsection we present an exploratory comparison between the tidal-averaged dissipation rates for the five anchor stations and turbulence energy estimates

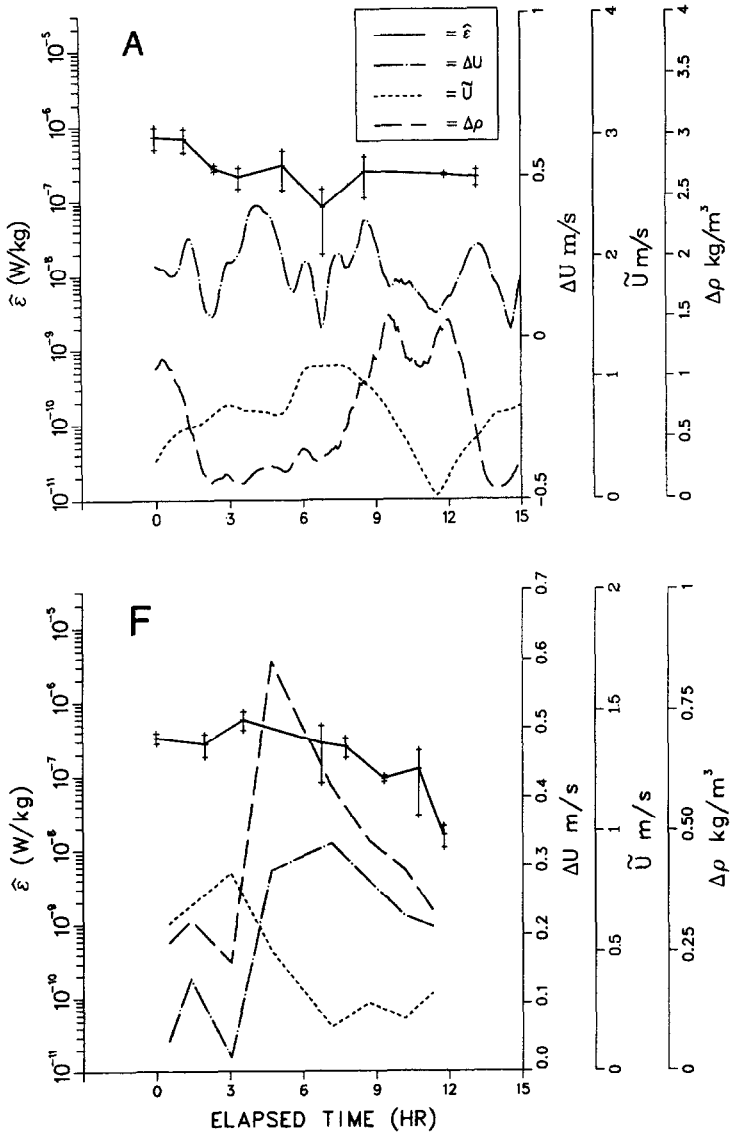

Fig. 12. Time series plots of the vertical/burst-averaged dissipation rates ($\hat{\varepsilon}$), magnitude of depth-averaged current ($\tilde{U}$), magnitude of vertical difference in velocity (ΔU) and vertical density difference ($\Delta\rho$) for anchor stations A and F. The dissipation rates are for the 9–35 m vertical interval, and the indices are for the 13–33 m interval for A (based on the moored measurements) and for the 20–40 m interval for F (otherwise as in Fig. 7).

from two three-dimensional (3-D) numerical models of summertime mean and semidiurnal tidal circulation on Georges Bank.

The first model is the diagnostic eddy-viscosity model of Naimie *et al.* (1994), which uses an iterative harmonic method to provide 3-D nonlinear solutions for the M_2 tidal and seasonal-mean flow components on realistic Georges Bank geometry, under observed

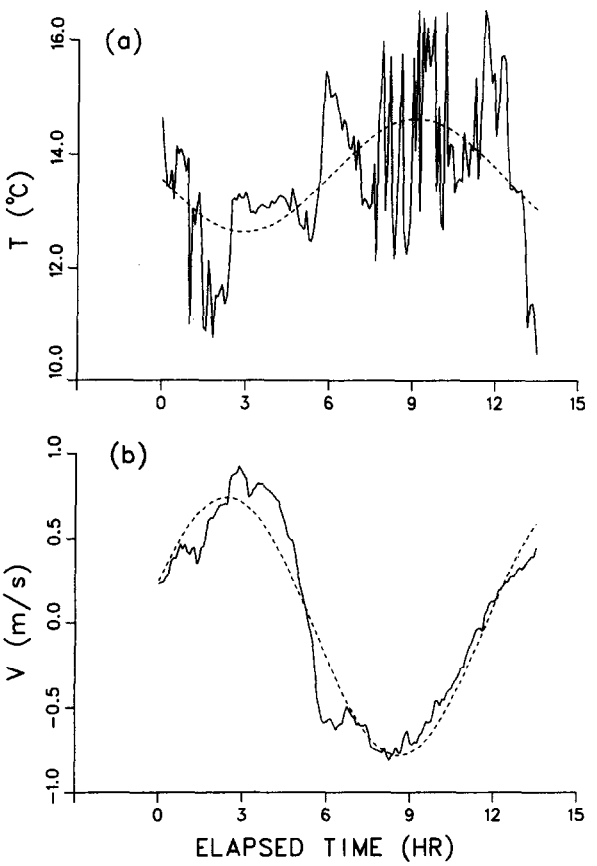

Fig. 13. Time series plots of (a) temperature and (b) north–south current (positive north) from the 13-m moored meter during anchor station A. The dashed lines are the associated "tidal" variations from regression fits of a constant term plus 12.4-h sinusoid.

forcing by M_2 tides and climatological-mean density and wind stress fields. Internal friction is represented through a time- and space-varying vertical eddy viscosity, N, which depends on the square of the vertically-averaged current magnitude and on a vertically-varying function (Munk and Anderson, 1948) of the local Richardson Number. For the comparison we choose the July–August solution (Figs 10(d) and 11(d) in Naimie *et al.*, 1994), and use model current and eddy viscosity profiles for ("similar h") nodes near our observation sites and with water depths (51.8/63.6 m for the mixed/frontal node) approximating those observed. The model profiles of tidal current amplitude and mean current are included in Figs 2 and 8, on the panels for anchor stations (D and A, respectively) with predicted tidal elevations (Yarmouth, N.S.) close to those in the model. The current agreement is very good considering the limited observation period, and the smoothed topography, climatological forcing and turbulence parameterization in the model. Predictions for the other anchor stations can be obtained by scaling the model currents by the predicted (Yarmouth) elevation ratios (Table 1), and confirm (at least) qualitative agreement of the observed currents with the monthly/fortnightly tidal modulation.

As an indicator of the turbulence levels implied by the eddy-viscosity model solution, we compute the tidal-averaged production rate of turbulent kinetic energy associated with the time-independent component $\mathcal{N}_m$ of the eddy viscosity (neglecting the effects of time-varying $\mathcal{N}$ and substantially simplifying the computation). This quantity is estimated as

$$\mathrm{TKEP}(z) = \rho \mathcal{N}_m \langle (\frac{\partial U}{\partial z})^2 + (\frac{\partial V}{\partial z})^2 + (\frac{\partial \bar{u}}{\partial z})^2 + (\frac{\partial \bar{v}}{\partial z})^2 \rangle \quad (1)$$

where ρ is density, (U, V) is the horizontal tidal current, $(\bar{u}, \bar{v})$ the horizontal mean current, and the angle brackets ($\langle\rangle$) denote time-averaging over the tidal period. It is usually assumed that this is the primary source term in the turbulent kinetic energy equation for both stratified and unstratified shear-driven turbulence, and that this term is approximately balanced by the turbulence dissipation rate, estimated here from our microstructure measurements.

The second model is the comprehensive prognostic model of Lynch *et al.* (in press) and Naimie (1995, 1996), which has an advanced turbulence closure following Mellor and Yamada (1982). For the comparison, we choose the climatological July–August solution presented in Naimie (1996), in which there has been advective and diffusive evolution of the Naimie *et al.* (1994) July–August density field under the same dynamical forcing and on the same topography as in the diagnostic eddy-viscosity model. The current profiles from the (similar h) selected model nodes are similar to those in the eddy-viscosity model, in approximate agreement with those observed (Figs 2 and 8). In contrast to the eddy-viscosity model, the advanced closure model provides direct estimates of the turbulent kinetic energy dissipation rates which can be compared with those measured.

We consider first the vertical distributions of tidal-averaged dissipation rate, $\tilde{\varepsilon}_m$, from the advanced model and of TKEP from the eddy-viscosity model, which are included on the tidal-averaged profile plots of measured dissipation rate for the various anchor stations (Figs 6 and 11). The model predictions are the values at the "similar h" nodes (obtained from the turbulence kinetic energy equation or (1)), adjusted for depth (h) differences between the model and field by assuming that $\tilde{\varepsilon}_m$ (or TKEP) $\propto h^{-3}$, and for the monthly/fortnightly tidal modulation by assuming that $\tilde{\varepsilon}_m$ (or TKEP) $\propto \Delta\zeta^3$ where $\Delta\zeta$ is the predicted elevation range at Yarmouth during the anchor station (Table 1). For the frontal stations, adjusted $\tilde{\varepsilon}_m$ profiles (from the advanced model) are included (Fig. 11) for a second ("same lat./long.") model position which has the same horizontal position as the observation site but a different water depth (76.8 m). As a quantitative comparison, the vertically-integrated and tidal-averaged rates for the vertical observational intervals at each station are included in Table 2 together with the measured rates.

The model-derived estimates of turbulence production and dissipation are generally within a factor of 2–3 of those observed, and have similar vertical structure in the interior water column. However, there are some significant differences: between the eddy-viscosity and advanced model estimates, between the two (advanced) model positions near the frontal site, and compared to the observed profiles. Whereas the eddy-viscosity model rates have a large decrease at the surface and limited vertical structure in the lower water column at the mixed site, the dissipation rates in the advanced model increase in the immediate vicinity of the sea surface and throughout the lower water column. The latter structure is more realistic for the bottom boundary layer, pointing to a deficiency in the assumed near-bottom eddy-viscosity structure in Naimie *et al.* (1994). Also, for the "similar h" node near the frontal site, the advanced model has turbulence levels about three times higher than the eddy-viscosity

Table 2. Comparison of tidal-averaged dissipation rates from microstructure measurements during the five anchor stations with the turbulence energy levels in the 3-D numerical circulation models of Naimie et al. (1994) *and Naimie* (1996), *and with estimates of wind energy input*

	A	B	D	E	F
Water depth (m)	63	48	53	55	63
Vertical observation interval (m)	9–41	9–29	9–39	9–39	9–41
Average measured dissipation rate ($\times 10^{-7}$ W/kg)	3.4	46	22	15	2.3
Vertically-integrated rates (W/m^2)					
Measured dissipation	0.011	0.091	0.066	0.044	0.007
Turbulence energy production in NLL94 model	0.012	0.031	0.059	0.018	0.004
Dissipation in N96 model: similar h	0.037	0.028	0.058	0.018	0.012
Dissipation in N96 model: same lat./long.	0.008	—	—	—	0.003
Wind energy input	0.010	0.083	0.014	0.001	0.001

The measured dissipation rates are presented as vertical averages and integrals over the vertical observation interval. The turbulence energy production rates in the Naimie *et al.* (1994; NLL94) model are the contributions associated with the time-independent components of $\mathcal{N}$ in the tidal and mean flow fields for July–August under forcing by M_2 tides, mean density and mean wind stress, adjusted for depth and tidal modulations. The turbulence dissipation rates in the corresponding Naimie (1996; N96) model solution are shown for the same model nodes (similar h) used in the NLL94 comparison and for the actual position (same lat./long., but different h) of the frontal site. The wind energy input rates are for the whole water column.

model. This occurs because of reduced stratification at this site in the prognostic solution, illustrated by the substantially-reduced dissipation rates at the deeper, more stratified ("same lat./long.") position in the advanced model (Fig. 11, Table 2). For the mixed-site stations, the turbulence estimates in both the eddy-viscosity and advanced models are: substantially lower than those observed at B consistent with an (additional) important contribution from the strong winds during this station, in approximate agreement with the observed dissipation rates at D (the station requiring the smallest depth/modulation adjustment), and substantially lower than the observed rates at E (possibly due to the crudeness of the large depth/modulation adjustment at this station). For the frontal-site stations, the eddy-viscosity model profiles are close to those observed at A and and in the lower water column at F, while the advanced model profiles from the two selected positions generally bracket the observed values for both A and F. Considering the uncertainties in our depth/modulation adjustment and the strong sensitivity to position in the frontal zone, we conclude that the observed and predicted tidal-averaged rates are in approximate agreement for both models, except during B (when winds were much stronger than in the model).

To provide a first indication of the consistency between the observed temporal variability over the tidal period and that in the advanced turbulence model, we show in Fig. 14 the t–z variations of model dissipation rate for the mixed and frontal sites (using the "same lat./long." position for the latter). The dissipation magnitudes have been adjusted (as described

Fig. 14. Time–depth plots of dissipation rate at the mixed (upper panel) and frontal (lower panel) sites from the Naimie (1996) model with advanced turbulence closure. The model values have been adjusted for depth and tidal modulation differences by the factors 1.1 and 1.81 appropriate to stations D and A, respectively. For the frontal site, the "same lat./long." model position is used, providing closest agreement with the observations (Fig. 11). Note that the distributions are shown for the entire water column, in contrast to the limited observational window (Figs 5 and 10).

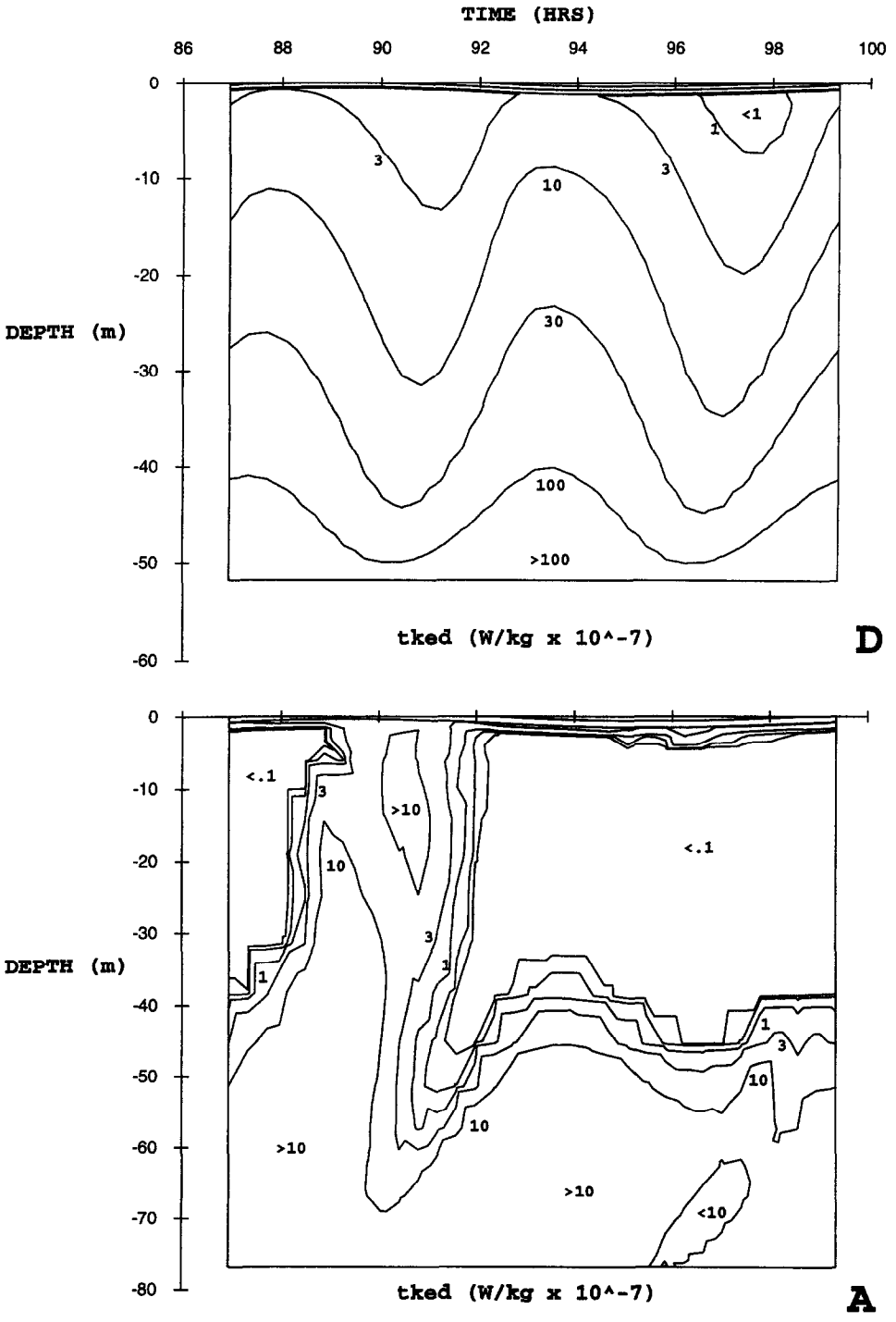
TIME (HRS)
86
88
90
92
94
96
98
100
0
-10
-20
-30
-40
-50
-60
DEPTH (m)
<1
1
3
3
10
30
100
>100
tked (W/kg x 10^-7)
D
0
-10
-20
-30
-40
-50
-60
-70
-80
DEPTH (m)
<.1
3
>10
10
<.1
3
1
1
1
3
10
10
>10
>10
<10
tked (W/kg x 10^-7)
A

above) for water depth and the tidal modulation during stations D and A, respectively. At the mixed site (Fig. 14(a)), the model variation shows similar qualitative structure to the observed variations during stations D and E (Fig. 5) with two maxima per period, although there is some suggestion that the magnitude of the temporal variation is smaller than observed. In contrast, the model variation at the frontal site is dominated by a large increase in dissipation throughout the water column during the phase of the tide when the strong eastward mean flow (Fig. 8) reinforces the tidal current and when there is minimal stratification at this site (due to tidal advection). Such a strong maximum is not apparent in the frontal-site observations (Fig. 10), probably in part because of the additional complicating influence of internal waves, but also pointing to the need for more detailed comparison between model turbulence variations and frontal observations. The frontal-site model variation also indicates that the present vertical observation interval only marginally overlaps with the turbulent bottom boundary layer during much of the tidal period, so that a more detailed observational evaluation of the model would be better done with an observational dataset that extends to the seafloor (e.g. Yoshida and Oakey, 1996). The t–z variation (not shown) at the (less stratified) "similar h" model node is qualitatively similar to that in Fig. 14(b), with magnitudes reduced by a factor of about 4.

Overall, this exploratory comparison provides encouraging support for the present dissipation rate estimates being reliable within expected uncertainties and for both circulation models having reasonable turbulence levels in the interior of the water column. However, there is also a clear indication that the advanced model has a more realistic turbulence representation (than the eddy-viscosity model) over the whole water column. A more thorough comparison with larger datasets is required to address properly the degree of quantitative consistency with the models and the physical mechanisms controlling the turbulence distributions, particularly in the complex frontal zone.

Influence of wind forcing

The measurements of wind speed during the anchor stations allow a crude estimation of the contribution of wind forcing to the measured dissipation rates. Assuming that the rate of wind energy input to the ocean, D_W, is a fraction γ of the rate of energy transfer across the 10-m (above sea surface) level, we take the tidal-averaged rate of wind energy input as

$$\langle D_W \rangle = \gamma \rho_a c_{10} \langle U_{10}^3 \rangle, \tag{2}$$

where ρ_a is the density of air, c_{10} a drag coefficient taken as 1.5×10^{-3}, and U_{10} the wind speed at 10 m. The appropriate value of γ is uncertain, but previous estimates are in the range 0.004–0.09 (Richman and Garrett, 1977; Oakey and Elliott, 1982; Moum and Caldwell, 1985; Oakey, 1985). As an estimate of the wind energy input, we include in Table 2 values of $\langle D_W \rangle$ for $\gamma = 0.02$, which indicate much larger wind energy input during B than the other stations. Comparison with the vertically-integrated dissipation rates for the observation intervals (Table 2), however, indicates that wind energy input was potentially a major factor during both stations A and B (although it should be noted that the present wind energy estimates are for the entire water column, whereas the dissipation observation intervals were typically about one-half of the water depth).

In principle, with dissipation rate measurements from three anchor stations at the mixed site under different tidal and wind forcings, it should be possible to quantify the contributions from tidal and wind energy with assumptions on the functional relation

between energy input rate and tidal current strength and/or wind speed. For example, if we assume that the tidal forcing is proportional to $\Delta\zeta^3$ (preceding subsection) and the wind forcing to $\langle U_{10}^3 \rangle$, then the tidal- and vertical-averaged dissipation rates for a common interval at the three stations yields three linear equations in two unknowns (coefficients for tidal and wind forcing). With these assumptions, the measured dissipation rates for stations B and D suggest that wind forcing accounts for 73% and 28%, respectively, of the total in the 9–29 m interval at these stations, while the rates for B and E suggest that wind forcing accounts for 39% and 4%, respectively, of the total at these stations. The difference in the two estimates for B probably reflects inappropriate assumptions on the functional relations and/or inaccuracies in the wind energy estimates. Nevertheless, the observations collectively suggest that wind forcing accounts for about half of the dissipation rate in the 9–29 m interval during B, and only a small fraction of the dissipation rate during stations D and E. If all of this wind contribution to dissipation rate applies to the upper 29 m of the water column (with no wind contribution below), then the above partitioning implies a value of γ near 0.02, our assumed value. The above estimates thus provide consistent support for significant contributions from both tides and wind to vertical mixing in the upper water column on central Georges Bank. However, since the average current speed (0.6 m/s) during station D is close to the average tidal current speed on the Bank (e.g., Butman *et al.*, 1982), while the average wind speed during D slightly exceeds the typical summertime wind speed (6 m/s) (Saunders, 1977), the estimates also support tidal mixing being the primary factor in the maintenance of vertically-mixed conditions through summer.

The present dataset is not adequate to resolve the contribution of wind forcing to mixing in the frontal zone, except that wind influences were insignificant during station F (Table 2).

Vertical diffusivities in frontal zone

From the t–z evolution of dissipation rate and density structure over the tidal period at the frontal site, we can estimate the variation in vertical eddy diffusivity K using the conventional scaling (e.g. Osborn, 1980) for diffusivity in a stably stratified fluid:

$$K = \Gamma\varepsilon/N^2. \tag{3}$$

Here, Γ is an empirical constant taken as 0.24 after Oakey (1982) and N is the Brunt–Vaisala frequency, which we approximate by $N^2 = -(g/\rho_o)\partial\rho/\partial z$, where g is gravitational acceleration. Using the burst-averaged dissipation rates averaged across 5–10 m vertical bins and the Brunt–Vaisala frequency based on the CTD density gradient across each bin, the t–z evolution shown in Fig. 15 is computed for K during anchor stations A and F. Values are generally in the range of (0.5–20) $\times 10^{-4}$ m^2/s^1, with a strong temporal variation over the tidal period and magnitudes generally increasing with depth at both stations. The tidal-averaged values are typically 2–3 times larger for A than F, illustrating the significant variation in vertical mixing associated with the monthly/fortnightly tidal modulation on Georges Bank.

The moored current and density measurements for station A allow comparison of the eddy diffusivities inferred from the microstructure measurements with those estimated from literature parameterizations. Loder *et al.* (1988) used the frontal-site moored measurements and a parameterization involving an Ekman layer approximation (Csanady, 1976) for the stratification-independent part of the diffusivity, and gradient Richardson number approximations (Munk and Anderson, 1948; James, 1977) for stratification influences to

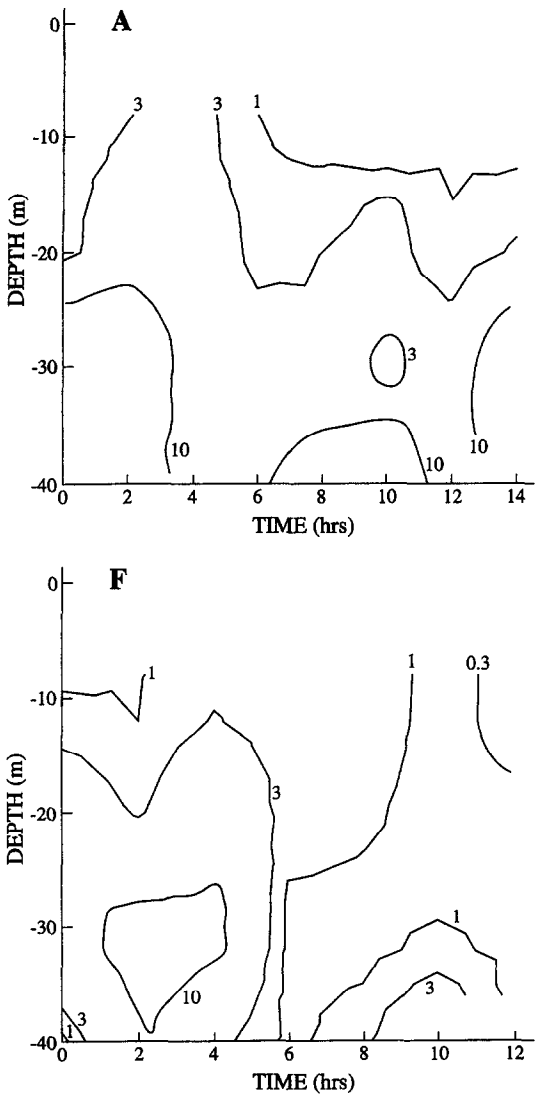

Fig. 15. Time–depth plots of the vertical eddy diffusivity ($\times 10^{-4}$ m^2/s) for anchor stations A and F, computed from equation (3).

estimate average magnitudes of (60–300) $\times 10^{-4}$ m^2/s^1 for K in the 13–33 m interval over the 2-week mooring period. While the temporal variability of K estimated from this parameterization shows qualitative similarity to that estimated from the microstructure measurements, the above magnitudes are about an order of magnitude larger than the average values of (3–8) $\times 10^{-4}$m^2/s^1 estimated from the microstructure observations in the corresponding vertical bins. This comparison suggests that the parameterization used in Loder *et al.* (1988) substantially overestimates the diffusivity away from the near-bottom region in the presence of moderate stratification, pointing to the need for careful observational validation of parameterizations of vertical mixing.

COMPARISON OF VERTICAL NITRATE FLUX WITH BIOLOGICAL DEMAND

Biological demand

Primary production measurements made concurrently with the microstructure measurements indicate that there is enhanced "new" production (i.e. based on inorganic nitrogen) in the tidal front on northern Georges Bank (Horne *et al.*, 1989). An important question is the physical pathway and mechanism for the supply of inorganic nutients from the deep waters surrounding the Bank to the frontal euphotic zone. Horne *et al.* (1989) showed that the measured cross-frontal (horizontal) flux of nitrate was adequate to meet the nitrogen requirements of the frontal zone and mixed area in a depth-integrated sense. With the diffusivity estimates from the microstructure measurements, we can now compare the vertical nitrate flux in the frontal zone with that required by the primary production.

The primary production measurements included vertical profiles of the rates of carbon assimilation (^{12}C method), and nitrate and ammonia uptake (^{14}N method) from six stations at the frontal site during the 20-day study period (see Table 1 of Horne *et al.* (1989) where these stations are referred to as "edge-of-bank"). The average value of the euphotic-zone integral of carbon assimilation rate during these stations was 5.4 gC/m^2/day, and that of the nitrate uptake rate was 2.8×10^{-4} mg at N/m^2/s. The average value of the *f*-ratio, the ratio of nitrate uptake rate to nitrate + ammonia uptake rate, was 0.53. Two of the stations were during anchor station A, while one of the stations was during anchor station F. The latter station had the lowest euphotic-zone integral values of carbon assimilation rate (2.6 gC/m^2/day), nitrate uptake rate (1.1×10^{-4} mg at N/m^2/s) and *f*-ratio (0.23). The average values of these variables during anchor station A were 5.3 gC/m^2/day, 2.8×10^{-4} mg at N/m^2/s, and 0.59, respectively.

Vertical flux of nitrate

Using the $K(z,t)$ values estimated earlier (Fig. 15) and the nitrate measurements (Fig. 16(a),(b)) taken during the CTD profiles, the vertical nitrate flux can be estimated as $K\Delta N'/z$ for the two frontal-site anchor stations (Fig. 16(c),(d)). Here, $\Delta N'$ is the difference in nitrate concentration across the vertical intervals for which K was computed. The estimated flux shows a strong variation over the tidal period, generally increased magnitude with increased depth, and reduced average magnitude during station F.

Light-meter observations during the primary production measurements (Horne *et al.*, 1989) indicate that the 1% light level (taken as the euphotic-zone depth) at the frontal site was about 40 m below the surface. The tidal-average nitrate flux at this level was 1.3×10^{-4} mg at N/m^2/s and 0.34×10^{-4} mg at N/m^2/s at stations A and F, respectively, only 30–46% of the estimated nitrate demand. Considering the limited datasets, the complexity of the frontal zone, and the associated uncertainties in the flux computations, the comparison of the estimated and required fluxes is encouraging, indicating an important contribution from vertical mixing to inorganic nutrient supply in the frontal euphotic zone. Both the estimated and required fluxes have reduced magnitudes during the weaker tidal forcing of station F, supporting variations in the nutrient supply associated with the tidal modulation (Bisagni and Sano, 1993). However, the substantial difference between the estimated and required fluxes suggests some combination of underestimation of the average turbulent flux, overestimation of the average demand, strong subtidal variability in the

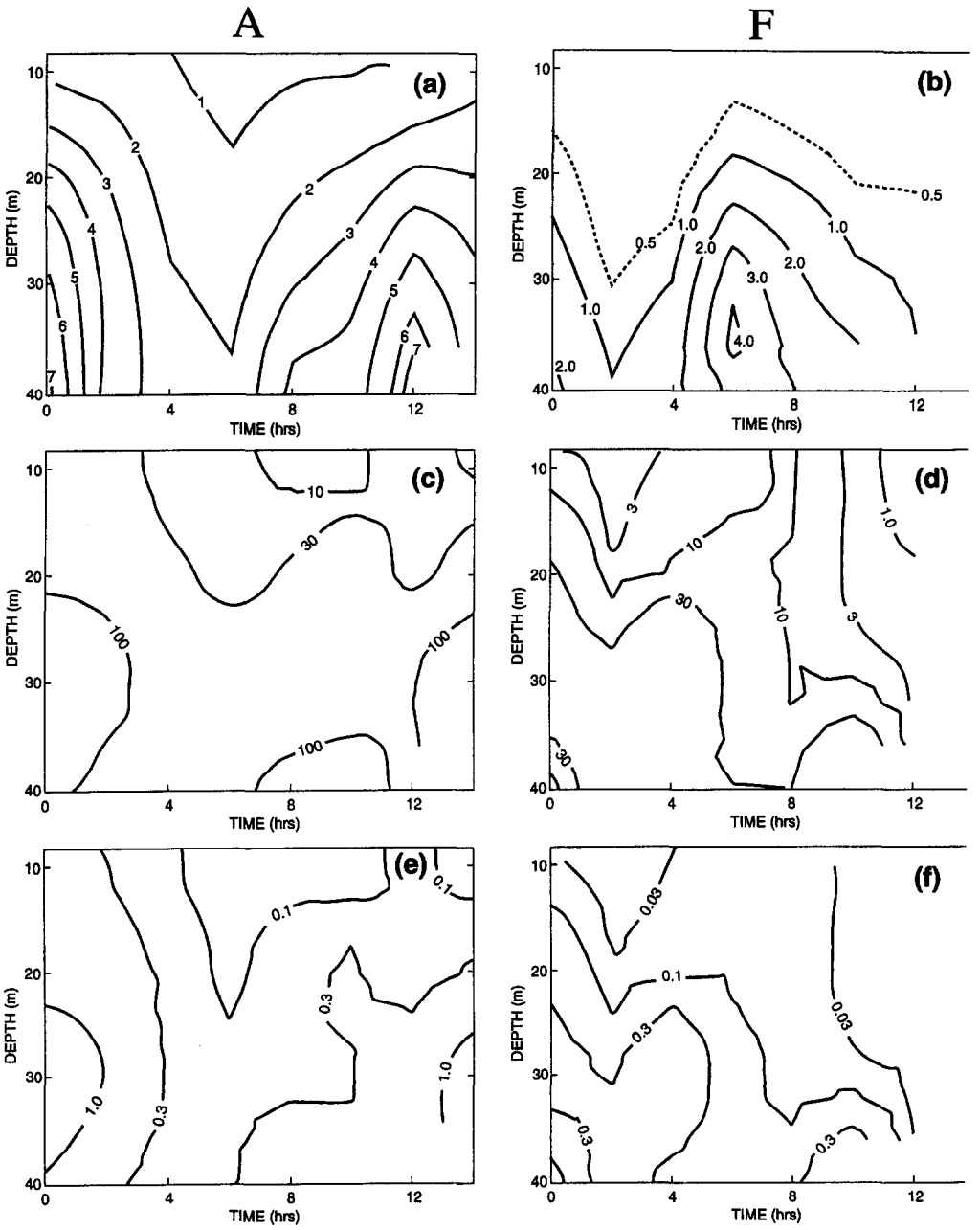

Fig. 16. Time–depth plots for anchor stations A and F of (a), (b) the nitrate concentration (mg at/m^3) from bottle samples at 10-m intervals, (c), (d) the vertical flux of nitrate ($\times 10^{-6}$mg at/m^2/s) estimated from the microstructure and CTD/nutrient measurements, and (e), (f) the integrated primary production rate (gC/m^2/day) in the overlying water which can be supported by the nitrate flux.

nitrate budget, and/or additional processes (e.g. upwelling or on-bank drift) contributing to the oceanic fluxes.

An alternative presentation of the nitrate flux estimates is the rate of (new) primary production (averaged across the overlying water) which the fluxes can support (Fig. 16(e),(f)), assuming the Redfield ratio for conversion of nitrogen to carbon. Averaged over the tidal period, the fluxes can support new production rates of 0.9 and 0.2 gC/m^2/day above 40 m during stations A and F, respectively. For both stations, the estimated rate is only about 30% of that implied by the measured carbon assimilation rates and *f*-ratios (e.g. $5.3 \times 0.59 = 3.1$ gC/m^2/day for A). A more extensive dataset of both biological and physical measurements is clearly required to resolve this discrepancy between the estimated vertical supply and biological demand rates. In particular, the differences in the biological measurements between the two stations during anchor station A (Table 1 of Horne *et al.*, 1989) point to the need for much more frequent biological sampling to resolve temporal variability in the frontal zone.

SUMMARY AND CONCLUSIONS

The dissipation rate measurements confirm that small-scale turbulence in the upper water column on Georges Bank has considerable spatial and temporal variability, including some regular variations and significant differences between the mixed area and stratified frontal zone. In the mixed area, in the absence of strong winds, there is a pronounced variation in the dissipation rate during the tidal period with two maxima each period, and an increase in the tidal-averaged rate with distance below the sea surface. The tidal variation is closely related to tidal variations in the current strength and vertical shear magnitude, supporting the tides as the primary forcing of the Bank's elevated vertical mixing rates.

The mixed-area observations are also consistent with longer-term variations in the upper ocean turbulence levels associated with both wind forcing and the monthly/fortnightly modulation of the tides (e.g. Bisagni and Sano, 1993). The dissipation rates increase markedly under moderate wind speeds, suggesting that the average tidal currents on Georges Bank and winds of 20–25 knots (about twice the summer average) make comparable contributions to the turbulence levels in the 9–29 m vertical interval. This supports Loder and Greenberg's (1986) and Bowers and Simpson's (1987) conclusions that a criterion for mixed-area extent involving wind, as well as tidal, mixing is appropriate.

The measurements in the frontal zone indicate weaker dissipation rates than in the mixed area by about an order of magnitude, a more complex temporal variation with no simple relation to the measured current and stratification variations, reduced vertical coherence of the temporal variability, and reduced vertical structure in the tidal-averaged rate in the upper water column. The weaker dissipation rates are consistent with a strong feedback in the dependence of dissipation rate on stratification, as previously suggested for tidal fronts (Simpson and Bowers, 1979). The origin of the more complex temporal variation is unclear, but the strong mean current in the frontal zone and internal waves originating at the Bank edge are likely contributors. The frontal zone contrasts the mixed area in that its turbulent bottom boundary layer is much more confined to the lower water column.

The favourable comparison with the turbulence levels in both the Naimie *et al.* (1994) and Naimie (1996) circulation models provides encouraging support for both the reliability of the measured dissipation rates and the potential of 3-D circulation models to predict turbulence levels at other times and locations. The dissipation variations in the Naimie

(1996) model with advanced turbulence closure indicate that both stratification and the frontal-zone mean flow may be important factors to the differences in vertical and temporal structure between the mixed and stratified sites. However, the limitations of the present observational dataset, together with the multiplicity of forcings on Georges Bank and the known nonlinearity of turbulence, point to the need for more detailed comparisons between models and expanded observational datasets.

The nitrate flux estimates indicate that vertical mixing is adequate to support new primary production rates of the order 0.5 $gC/m^2/day$ in the frontal euphotic zone on Georges Bank. The tidal-averaged flux at the base of the euphotic zone differs by a factor of about 4 between the two anchor stations, supporting a significant long-term variation in nutrient supply and primary production associated with the monthly/fortnightly tidal modulations (Bisagni and Sano, 1993). However, the estimated fluxes are only about one-third of the nitrogen demand estimated from the concurrent biological measurements (Horne *et al.*, 1989), pointing to the need for additional measurements to resolve the strong spatial and temporal variability in the frontal zone, and possibly an additional nutrient supply mechanism (e.g. upwelling).

While the present observations and analyses provide novel quantitative information on an important aspect of the physical environment on Georges Bank, it is clear that resolution of the plethora of physical and biological questions pertaining to vertical mixing on the Bank, and in tidally-energetic shallow seas in general, will require a progression of more extensive datasets and sophisticated analyses, interpreted in conjunction with advanced turbulence closure models.

Acknowledgements—We extend special thanks to Aaron Beazley for carrying out much of the data analysis, and to Glen Harrison for support and discussions during Hudson cruise 85020 and subsequently. We also thank Brian Irwin, Mark Hodgson, and the other scientific personnel for their help at sea and with the nutrient analysis; Dan Lynch, Justin Ip and Francisco Werner for their efforts in developing the circulation models; Mary Jo Graça for assistance with the model comparison; Jim Elliott, Brian Petrie, Trevor Platt and anonymous reviewers for helpful comments on earlier versions of the manuscript; and the late Captain Ross Dickenson and the officers and crew of the CSS Hudson for their patience and co-operation. This work was partially supported by the (Canadian) Federal Panel on Energy, Research and Development. This is contribution number 33 of the U.S. GLOBEC program, jointly funded by NSF and NOAA.

REFERENCES

Bigelow H. B. (1927) Physical oceanography of the Gulf of Maine. *Bulletin of the U.S. Bureau of Fisheries*, **40**, 511–1027.

Bisagni J. J. and M. H. Sano (1993) Satellite observations of sea surface temperature variability on southern Georges Bank. *Continental Shelf Research*, **13**, 1045–1064.

Bowers D. G. and J. H. Simpson (1987) On the mean position of tidal fronts in European shelf seas. *Continental Shelf Research*, **7**, 35–44.

Bowman M. J., A. C. Kibblewhite, S. M. Chiswell and R. A. Murtagh (1983) Shelf fronts and tidal stirring in Greater Cook Strait, New Zealand. *Oceanologica Acta*, **6**, 119–129.

Brickman D. and J. W. Loder (1993) The energetics of the internal tide on northern Georges Bank. *Journal of Physical Oceanography*, **23**, 409–424.

Butman B., R. C. Beardsley, B. Magnell, D. Frye, J. A. Vermersch, R. Schlitz, R. Limeburner, W. R. Wright and M. A. Noble (1982) Recent observations of the mean circulation on Georges Bank. *Journal of Physical Oceanography*, **12**, 569–591.

Csanady G. T. (1976) Mean circulation in shallow seas. *Journal of Geophysical Research*, **81**, 5389–5399.

Dewey R. K. and W. R. Crawford (1988) Bottom stress estimates from vertical dissipation rate profiles on the continental shelf. *Journal of Physical Oceanography*, **18**, 1167–1177.

Dewey R. K., W. R. Crawford, A. E. Gargett and N. S. Oakey (1987) A microstructure instrument for profiling oceanic turbulence in coastal bottom boundary layers. *Journal of Atmospheric and Oceanic Technology*, **4**, 288–297.

Garrett C. J. R., J. R. Keeley and D. A. Greenberg (1978) Tidal mixing versus thermal stratification in the Bay of Fundy and Gulf of Maine. *Atmosphere–Ocean*, **16**, 403–423.

Gurvich A. S. and A. M. Yaglom (1967) Breakdown of eddies and probability distributions for small-scale turbulence. *Physics of Fluids*, **10** Suppl., 559–565.

Harrison W. G., E. P. W. Horne, B. Irwin and T. Platt (1990) Biological production on Georges Bank: are tidal fronts primary sources of new production in summer? *EOS*, **71**, 96.

Hinze J. O. (1959) *Turbulence: An introduction to its mechanism and theory*. McGraw-Hill, New York, 586 pp.

Horne E. P. W., J. W. Loder, W. G. Harrison, R. Mohn, M. R. Lewis, B. Irwin and T. Platt (1989) Nitrate supply and demand at the Georges Bank tidal front. *Scientia Marina*, **53**, 145–158.

James I. D. (1977) A model of the annual cycle of temperature in a frontal region of the Celtic Sea. *Estuarine and Coastal Science*, **5**, 339–353.

Loder J. W. and D. A. Greenberg (1986) Predicted positions of tidal fronts in the Gulf of Maine region. *Continental Shelf Research*, **6**, 397–414.

Loder J. W. and E. P. W. Horne (1991) Skew eddy fluxes as signatures of nonlinear tidal current interactions, with application to Georges Bank. *Atmosphere–Ocean*, **29**, 517–546.

Loder J. W., C. K. Ross and P. C. Smith (1988) A space- and time-scale characterization of circulation and mixing over submarine banks, with application to the northwestern Atlantic Continental Shelf. *Canadian Journal of Fisheries and Aquatic Science*, **45**, 1860–1885.

Loder J. W., D. Brickman and E. P. W. Horne (1992) Detailed structure of currents and hydrography on the northern side of Georges Bank. *Journal of Geophysical Research*, **97**, 14,331–14,351.

Loder J. W., R. I. Perry, K. F. Drinkwater, J. Grant, G. C. Harding, W. G. Harrison, E. P. W. Horne, N. S. Oakey, C. T. Taggart, M. J. Tremblay, D. Brickman and M. M. Sinclair (1992b) Physics and biology of the Georges Bank frontal system. In: *Science Review* 1990 & 1991, T. E. Smith and J. Cook, editors, DFO, Dartmouth, N.S., pp. 57–61.

Loder J. W., K. F. Drinkwater, N. S. Oakey and E. P. W. Horne (1993) Circulation, hydrographic structure and mixing at tidal fronts: the view from Georges Bank. *Philisophical Transactions of the Royal Society of London, Series A*, **343**, 447–460.

Lynch D. R., J. T. C. Ip, C. E. Naimie and F. E. Werner (in press) Comprehensive coastal circulation model with application to the Gulf of Maine. *Continental Shelf Research*.

Mellor G. L. and T. Yamada (1982) Development of a turbulence closure model for geophysical problems. *Reviews of Geophysics and Space Physics*, **20**, 851–875.

Moum J. N. and D. R. Caldwell (1985) Local influences on shear-flow turbulence in the equatorial ocean. *Science*, **230**, 315–316.

Munk W. H. and E. R. Anderson (1948) Notes on a theory of the thermocline. *Journal of Marine Research*, **7**, 276–295.

Naimie C. E. (1995) On the modeling of the seasonal variation in the three-dimensional circulation near Georges Bank. Ph.D. Thesis, Dartmouth College, Dartmouth, Nova Scotia.

Naimie C. E. (1996) Georges Bank residual circulation during weak and strong stratification periods—prognostic numerical model results. *Journal of Geophysical Research*, **101**, 6469–6486.

Naimie C. E., J. W. Loder and D. R. Lynch (1994) Seasonal variation of the three-dimensional residual circulation on Georges Bank. *Journal of Geophysical Research*, **99**, 15,967–15,989.

Oakey N. S. (1982) Determination of the rate of dissipation of turbulent energy from simultaneous temperature and velocity shear microstructure measurements. *Journal of Physical Oceanography*, **12**, 256–271.

Oakey N. S. (1985) Statistics of mixing parameters in the upper ocean during JASIN phase 2. *Journal of Physical Oceanography*, **15**, 1662–1675.

Oakey N. S. (1988) EPSONDE: An instrument to measure turbulence in the deep ocean. *IEEE Journal of Oceanic Engineering*, **13**, 124–128.

Oakey N. S. and J. A. Elliott (1982) Dissipation within the surface mixed layer. *Journal of Physical Oceanography*, **12**, 171–185.

Osborn T. R. (1980) Estimates of the local rate of vertical diffusion from dissipation measurements. *Journal of Physical Oceanography*, **10**, 83–89.

Osborn T. R. and W. R. Crawford (1980) An airfoil probe for measuring velocity fluctuations in the water. In: *Air–sea interaction: Instruments and methods*, F. W. Dobson, L. Hasse and R. Davis, editors, Plenum Press, New York, pp. 369–386.

Perry R. I., G. C. Harding, J. W. Loder, M. J. Tremblay, M. M. Sinclair and K. F. Drinkwater (1993) Zooplankton distributions at the Georges Bank frontal system: retention or dispersion? *Continental Shelf Research*, **13**, 357–383.

Pingree R. D. (1978) Mixing and stabilization of phytoplankton distributions on the northwest European continental shelf. In: *Spatial pattern in plankton communities*, Vol. 3, J. H. Steele, editor, Plenum Press, New York, pp. 181–220.

Richman J. and C. J. R. Garrett (1977) The transfer of energy and momentum by the wind to the surface mixed layer. *Journal of Physical Oceanography*, **7**, 876–881.

Saunders P. M. (1977) Wind stress on the ocean over the eastern continental shelf of North America. *Journal of Physical Oceanography*, **7**, 555–566.

Schumacher J. D., T. H. Kinder, D. J. Pashinski and R. L. Charnell (1979) A structural front over the continental shelf of the eastern Bering Sea. *Journal of Physical Oceanography*, **9**, 79–87.

Simpson J. H. (1981) The shelf-sea fronts: implications of their existence and behaviour. *Philosophical Transactions of the Royal Society of London, Series A*, **302**, 531–546.

Simpson J. H. and J. H. Hunter (1974) Fronts in the Irish Sea. *Nature*, **250**, 404–406.

Simpson J. H. and D. Bowers (1979) Shelf sea fronts' adjustments revealed by satellite IR imagery. *Nature*, **280**, 648–651.

Simpson J. H. and J. Sharples (1994) Does the Earth's rotation influence the location of the shelf sea fronts? *Journal of Geophysical Research*, **99**, 3315–3319.

Simpson J. H., D. G. Hughes and N. C. G. Morris (1977) The relation of seasonal stratification to tidal mixing on the continental shelf. In: *A voyage of discovery, Supplement to Deep-Sea Research*, M. Angel, editor, Pergamon Press, Oxford, pp. 327–340.

Soulsby R. L. (1983) The bottom boundary layer of shelf seas. In: *Physical oceanography of coastal and shelf seas*, B. Johns, editor, Elsevier Science Publishers, Oxford, pp. 189–266.

Tremblay M. J. and M. Sinclair (1992) Planktonic sea scallop larvae (*Placopecten magellanicus*) in the Georges Bank region: broadscale distribution in relation to physical oceanography. *Canadian Journal of Fisheries and Aquatic Science*, **49**, 1597–1615.

Veth C. (1990) Turbulence measurements in the tidally mixed Southern Bight of the North Sea. *Netherlands Journal of Sea Research*, **25**, 301–330.

Yamazaki H. and R. Lueck (1990) Why oceanic dissipation rates are not lognormal. *Journal of Physical Oceanography*, **20**, 1907–1918.

Yoshida J. and N. S. Oakey (1996) Characterization of vertical mixing at a tidal-front on Georges Bank. *Deep-Sea Research II*, **43**, 1713–1744.